Russian Geology and Geophysics
Vol. 47, No. 10, pp. 1056-1070, 2006

Geologiya i Geofizika
UDC 550.831.016+550.357.64(571.53.53/.55+517.4)

THE NATURE OF CENOZOIC UPPER MANTLE PLUMES IN EAST SIBERIA (*Russia*) AND CENTRAL MONGOLIA

Yu.A. Zorin, E.Kh. Turutanov, V.M. Kozhevnikov, S.V. Rasskazov, and A.I. Ivanov

Institute of the Earth's Crust, Siberian Branch of the RAS, 128 ul. Lermontova, Irkutsk, 664033, Russia

We discuss the space relationship between upper mantle plumes revealed earlier from analysis of long-wavelength isostatic gravity anomalies and the subducting Pacific slab. According to global seismic tomography, the oceanic slab in its segments corresponding to the Japan and Izu–Bonin island arcs flattens out at the bottom of the mantle transition zone, extends horizontally far beneath Eurasia, and then resumes sinking into the lower mantle. The upper mantle plumes are located beyond the western endpoint of the slab sector that advances the farthest beneath the continent.

A considerable part in the plume material may belong to fertilized (enriched with incompatible elements) peridotite. A layer of fertilized peridotite forms at depths between 200 and 600 km under the effect the melts produced by partial melting of the slab oceanic crust cause on the overlying depleted mantle. The peridotite layer integrates into the slab and heats up by friction along the slab top during the horizontal motion of the latter in the transition zone where the mantle material is of relatively high strength. Portions of hot fertilized peridotite detach from the slab as it sinks into the lower mantle, rise by buoyancy through the upper part of the transition zone, and become entrained into an elongate asthenospheric convection cell which arises beneath the continent behind the subduction zone. The ascending convection flow splits into separate streams which are the upper mantle plumes.

Upper mantle plumes, subducting slab, mantle transition zone, fertilized peridotite, asthenospheric convection

INTRODUCTION

The concept of mantle plumes has been often invoked through the recent fifteen years to explain the specific features of Cenozoic magmatism in East Siberia and Central Mongolia as well as the geodynamics of the Baikal rift zone [1–7]. Yet the position and the geometry of Cenozoic plumes remained unclear. We proposed [8, 9] to detect and locate plume tails using long-wavelength isostatic gravity anomalies proceeding from the assumption that low viscosity in the asthenosphere almost eliminates the effect of the plume-related mass deficit on the Earth's surface topography. We constructed several gravity models of plume tails beneath the Baikal rift and beneath mountains of Central Mongolia. The predicted location of plume tails agrees well with the distribution of long-period Rayleigh group velocities and with azimuthal seismic anisotropy data [8, 9].

Although the idea of the plume geometry and size we obtained is very tentative, the quite low intensity of the related gravity anomalies and possible variation range of the mass deficit suggest that the plume tails occur within the upper mantle [9, 10]. There is an opinion that only the ascending flows that rise from the D″ layer at base of the lower mantle would be referred to as plumes [11]. However, plumes can arise in upper mantle as well [12–14] and it appears thus reasonable to call them upper mantle plumes.

Some recent studies attribute Cenozoic basaltic volcanism in southern East Siberia, Central Mongolia, and Northeastern China to the specific behavior of the Pacific subduction in its segments corresponding to the Japan and Izu–Bonin island arcs [15, 16]. According to global seismic tomography [17–20], the subducting Pacific plate, which shows up as a high-velocity zone, flattens out in the mantle transition zone (at depths between 420 and

660 km) and extends horizontally beneath Eurasia above the 660 km discontinuity for more than 1500 km as far as Eastern Transbaikalia and Eastern Mongolia, where eventually sinks into the lower mantle. The flat-lying plate segment is termed *stagnated* or *stagnant slab* in the modern geological and geophysical literature. Strictly speaking, the term *stagnation* should refer rather to a fixed depth position than to absolute immobility of the plate: Otherwise, without horizontal motion, the plate would never advance as far beneath the continent.

It was hypothesized that dehydration of hydrosilicates preserved in the stagnant slab provides fluid supply to the asthenosphere, which causes ascending convection flow and the related upwelling of the asthenosphere [15]. The progress of upwelling gives rise to basaltic magmas and rifting. The center of the upwelling was presumed to occur in Northeastern China and basaltic fields in East Siberia and Central Mongolia to fall on its northwestern periphery [15]. Below we show that the hypothesis of an ascending asthenospheric flow with its center in Northeastern China contradicts gravity data, namely the absence of long-wavelength gravity lows. Negative gravity anomalies exist within an area that covers southeastern East Siberia and Central Mongolia, where we predict the location of upper mantle plumes [9, 10].

On the other hand, numerical [21] and laboratory [22] modeling experiments showed in the early 1980s, when no evidence on slab stagnation was available, that the cooling effect from a subducting plate can cause upper mantle convection in up to 3000–4000 km elongate cells. According to Froidevaux and Nataf [22], a convection cell may exist beneath the East Asian lithosphere, with its descending flow at the Pacific subduction zone and the ascending flow beneath the Baikal rift.

Questions naturally arise whether the upper mantle plumes we discovered may be associated with the ascending convection flow and which may be their relation to the stagnant Pacific slab. In this paper we try to approach the solution to these problems and gain an insight into the nature of upper mantle plumes using geophysical data combined with the available knowledge of the composition of upper mantle and processes in it.

1. GEOPHYSICAL DATA ON THE SPACE RELATIONSHIP BETWEEN THE STAGNANT PART OF THE PACIFIC SLAB AND UPPER MANTLE PLUMES

Global seismic tomography [20] (Fig. 1) gives an idea of the position of the stagnant part of the oceanic slab beneath East Asia. See the distribution of velocity anomalies $(100\Delta V_P/V_P)\%$ at a depth of 550 km in the map and in the cross section along the line AB corresponding to the great-circle arc, where ΔV_P is the deviation of the computed *P*-wave velocity from its standard value V_P in the IASPI 91 model. We chose this tomography version because it accounts for refraction of seismic rays at the Moho and at the top and bottom of the mantle transition zone. Furthermore, velocity anomalies in the tomography version we use are obtained at grid nodes located at fixed depths (one in the lower half of the mantle transition zone) rather than in blocks (prisms). The digital data used to compile the map and the cross section are courtesy of Zhao [20].

Narrow high-velocity zones at a depth of 550 km record the slab segments sinking straight into the lower mantle without stagnation in the transition zone. According to *P*- and *S*-wave regional seismic tomography [19], the plate segments corresponding to the Kuriles-Kamchatka (northern part of the area of Fig. 1), Mariana, and Philippines (southern part, Fig. 1) subduction zones do not stagnate.

Broad high-velocity zones may record the flat-lying (depth-stagnant) slab part that remains connected to the modern subduction zone and continues subducting beneath the continent as well as older (now immobile) pieces of oceanic lithosphere which lost this connection. The latter include, for example, the plate remnant discovered beneath Chukotka by high-resolution seismic tomography [23]. It presumably lost its link with the moving oceanic lithosphere after the accretion of Kamchatka to Eurasia and the jump of the subduction zone from the continental margin to its modern position at the Kuriles-Kamchatka island arc.

The connection of the flat-lying slab part with the subduction zone can be checked against the continuity of high-velocity anomalies traceable from the point where the Wadati-Benioff seismic zone enters the mantle transition zone. This criterion is satisfied by the slab segments located northwest of the Japan and Izu–Bonin island arcs. The depth-stagnant slab part has the greatest extent (across the strike) in the segment related to the Japan arc (central part of the area of Fig. 1). The Japan and Izu–Bonin subduction zones are separated by transform faults which apparently continue beneath the continent, judging by flexural bending of the Wadati-Benioff zone surface [24]. The sectors of the oceanic lithosphere on both sides of the transform faults evolved following several different scenarios: The northern and southern segments may have included terranes with subcontinental lithosphere whose accretion caused changes in the subduction zone [25].

The upper mantle plumes we revealed from gravity data [8–10], as well as the related volcanic fields, group into an area located west of the central segment of the oceanic slab which advances the farthest beneath the

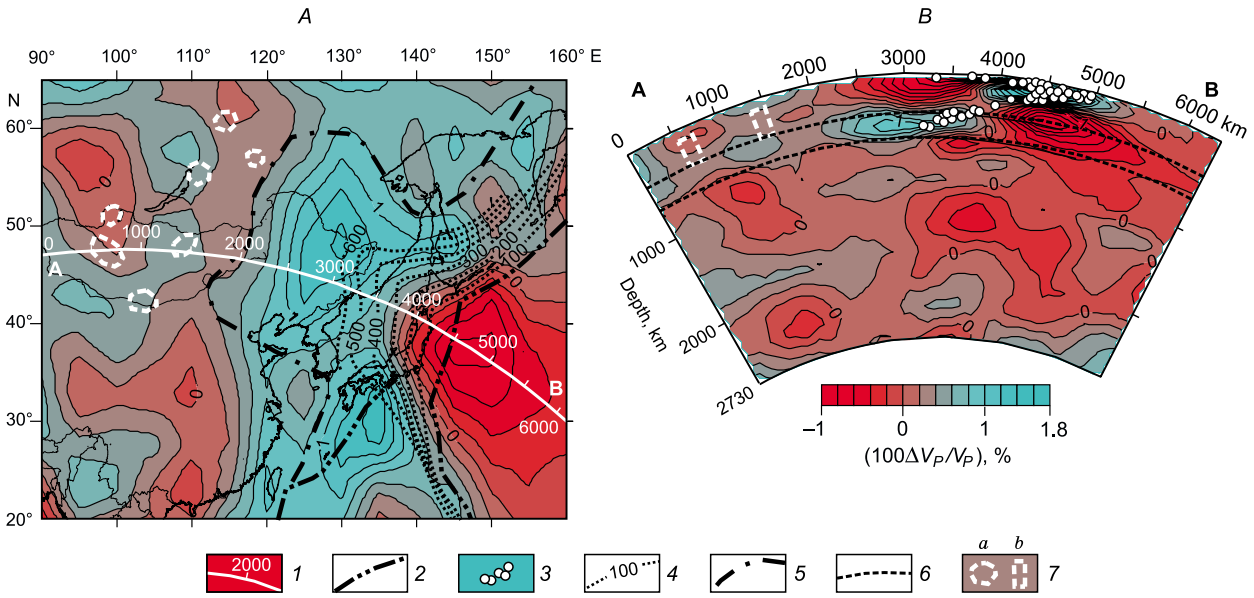

Fig. 1. Distribution of seismic velocity anomalies $(\Delta V_P/V_P)\cdot 100\%$ at depth 550 km (*A*) and cross section along line AB (*B*), from digital global seismic tomography [20]. *1* — cross section line (figures measure distance from beginning of profile, in km); *2* — axes of trenches; *3* — earthquake hypocenters; *4* — depth contour lines (km) of Wadati-Benioff seismic zone [24]; *5* — western boundary of the part of stagnant slab that remains connected with subduction zone; *6* — boundaries of mantle transition zone in cross section; *7* — upper mantle plumes: *a* — in map, *b* — in cross section (see model *C* in Fig. 3).

continent; this area extends in the direction roughly parallel to the edge of the high-velocity zone (Fig. 1). Global seismic tomography cannot resolve the plume tails, with their diameters under 200 km [14].

Slab sinking into the lower mantle is detectable in the cross section (Fig. 1, after [20]) at the western end of the stagnant segment. Note that slab sinking is more prominent in cross sections in [17, 18] where the totality of data and the specific methods provided a higher resolution of seismic tomography for vertically oriented objects.

It appears reasonable to correlate the seismic results with the field of long-wavelength (regional) isostatic gravity anomalies which reflect isostasy perturbation as well as the distribution of gravity masses below the level of isostatic compensation presumably located beneath continents at depths of ~150–200 km [9]. The plume tails were detected and located using relatively high-resolution gravity data from East Siberia and Mongolia processed with special techniques [8–10]. For the lack of high-resolution isostatic anomalies data for the whole territory of Fig. 1, we correlate the seismic data to the gravity field using global isostatic anomalies obtained in [26] in $1^\circ \times 1^\circ$ grid nodes from free air anomalies and topographic heights. The gravity anomalies in [26] are related to the geoid rather than to a spheroid as in our works. We applied $5^\circ \times 5^\circ$ sliding-window averaging (Fig. 2) to the digital data from [26], which roughly corresponds to the filtering we used earlier [9, 10].

The field of long-wavelength isostatic gravity anomalies in Fig. 2 notably differs in the average level from the anomalies we obtained for East Siberia and Mongolia (Fig. 3, *A*) because of the difference in the Earth geometry assumptions (spheroid and geoid). However, the position and relative intensity of the anomalies associated with the plume tails are similar in the two fields (cf. Figs. 2 and 3, *A*) despite the moderate resolution of the primary data used in [26] and the difference in the approaches to estimating the depth of compensation masses.

Figure 3 shows two gravity models of plume tails in order to illustrate some uncertainty associated with the interpretation of gravity anomalies. In both cases plume tails were simulated by vertical cylinders (polygonal prisms) following the techniques reported in [8, 9]. Note that the plume **heads** which fill asthenospheric upwarps participate in isostasy and their gravity effect was eliminated when calculating isostatic gravity anomalies. In the model *B*, the plume **tails** had their bottom at a depth of 670 km and the top at 200 km [9]. In the new model *C*, these depths are 420 and 150 km, respectively. The latter depth corresponds to the estimate of the maximum thickness of continental lithosphere east and south of the Siberian craton [10]. Tying the observed and computed

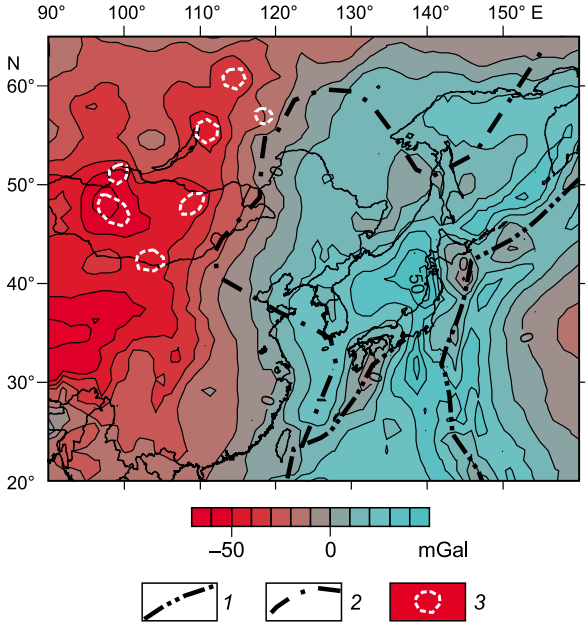

Fig. 2. Long-wavelength ($5° \times 5°$ sliding-window filtered) isostasy gravity anomalies. Initial anomaly fields after [26]. *1* — axes of trenches; *2* — western boundary of the part of stagnant slab that remains connected with subduction zone (see Fig. 1); *3* — upper mantle plumes (see model *C* in Fig. 3).

gravity field to an accuracy of ±4.5 mGal, with an assumed anomalous density of –20 kg/m^3, required adding 10.4 mGal to the computed anomalies in the model *B* and only 3.3 mGal in the model *C*. The lower area-constant correction indicates the advantage of the model *C*, as imposing too great depths for the plume bottoms in the case of relatively closely spaced bodies increases especially the long-wavelength components of theoretical gravity lows, these components being compensated by the added constant positive background. The advantage of *C* is further stressed by ideas we develop in Section 4 (see below). Note that the new model predicts almost the same locations of the plume tails and even the same sizes of their surface projections as in the model *B* (cf. panels *B* and *C* in Fig. 3). The revised depths of the plumes bottom does not change our basic inferences on the agreement between gravity and seismic data [9] and on the part of the plumes in the geodynamics of the Baikal rift [10].

The anomalies from separate plumes in the western part of the area of Fig. 2 merge into a zone of negative gravity which extends to the south where it bifurcates. The western arm falls into the territory of Tibet where the gravity low occupies the greatest area. Generally, the gravity lows apparently correspond to low-density upper mantle regions that tend to rise by buoyancy. No such gravity lows are observed in East China, between the plumes and the oceanic trenches (Fig. 2), which indicates the absence of ascending convection flow hypothesized in [15].

The trenches, currently seismically active, are marked by a series of gravity lows. These features of the gravity field, as well as the series of gravity highs over the oceanic rise east of the active trenches, are related to isostasy disturbance produced by slab pull into the subduction zone (Fig. 2). Linear gravity highs west of the trenches correspond to the inclined part of the subducting Pacific plate.

The depth-stagnant slab fits an area of relatively high gravity similar in geometry to the seismic high-velocity zone (cf. Figs. 1 and 2). Note that the gravity field bears signature of all parts of the stagnant slab (both connected to and separated from the modern subduction zone) as well as gravity-producing bodies located above and below the depth level imaged in the map of Fig. 1. Therefore, comparison of the two figures with regard to the latter note shows a rather good agreement between the gravity and seismic data.

Thus, the combined analysis of seismic and gravity data allows an inference that the area of upper mantle plumes to which we attribute the fields of within-plate basalts the most distant from the trenches is located near the edge of the flat-lying slab fragment which advances the farthest beneath the continent and continues moving. This fact appears not fortuitous.

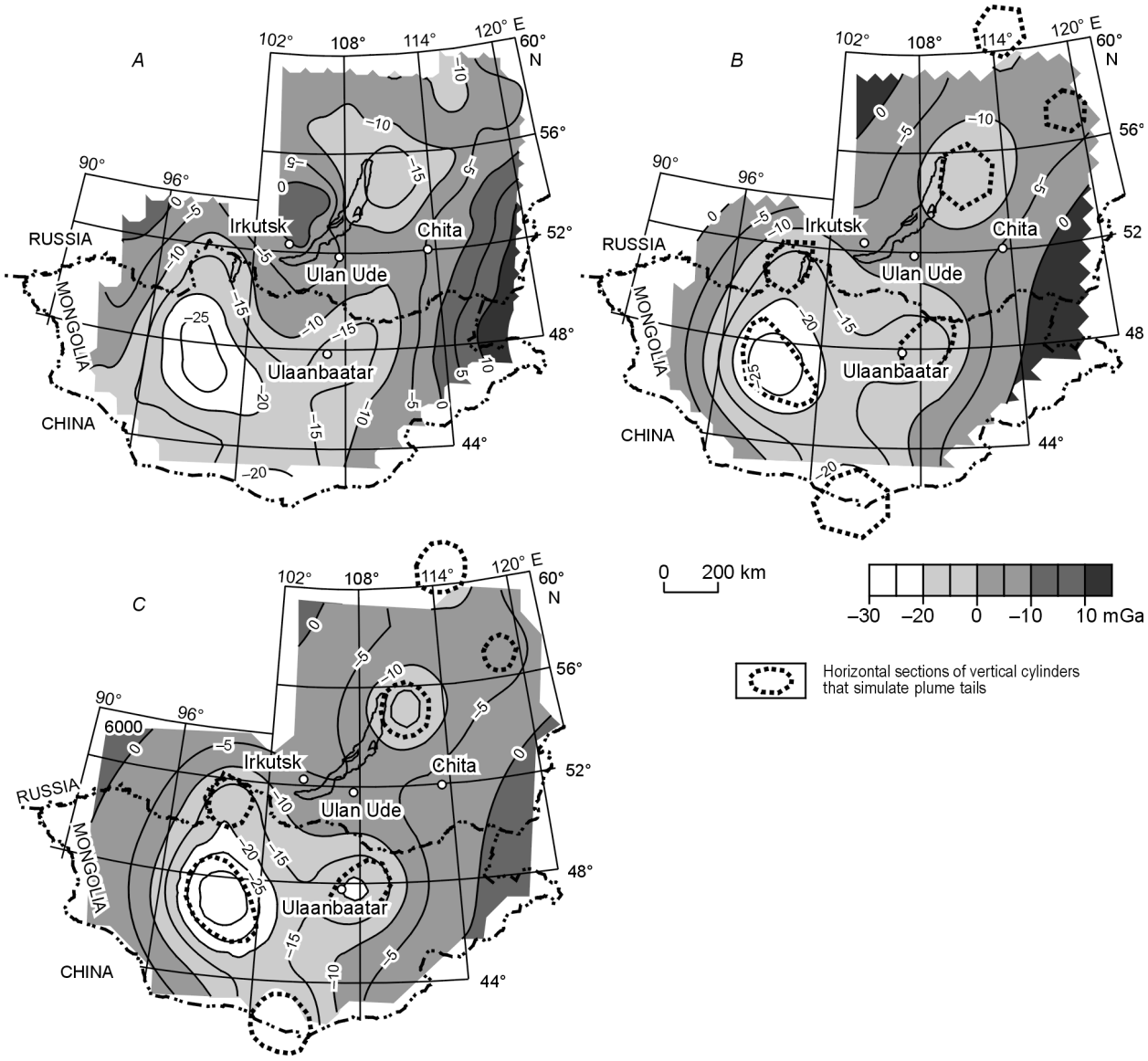

Fig. 3. Gravity models of plume tails. *A* — Long-wavelength isostasy gravity anomalies [8, 9]. *B* — Theoretical total gravity effect of vertical cylinders with their top at depth of 200 km and bottom at 670 km; 10.4 mGal added to theoretical anomalies [9]. *C* — Same effect but with top of cylinders at 150 km and their bottom at 420 km; 3.3 mGal added to theoretical anomalies. Both models assume density deficit of –20 kg/m^3, which corresponds to temperature increment of ~200 °C relative to ambient material.

2. DYNAMICS OF THE SUBDUCTING SLAB AND ITS DEPTH STAGNATION

The oceanic slab sinks in the subduction zone mainly because it is colder than surrounding mantle and is thus negatively buoyant. At the same time, compositional variations associated with phase change of olivine can give rise to additional petrological buoyancy forces [27–30].

Olivine (O) transforms into wadsleyite, its denser phase, at the top of the transition zone (at a depth of 420 km) in the normal mantle, and wadsleyite transforms into ringwoodite at about 520 km [29]. The two phases (wadsleyite and ringwoodite), being similar in density, are often considered jointly as a single phase and conventionally called “spinel” (Sp) [27, 30]. Spinel (olivine with spinel structure) presumably transforms into

denser magnesiowüstite (Mw) and ferromagnesian silicate perovskite (Pv) at the bottom of the transition zone at ~660 km [28, 29].

These phase transformations occur close to thermodynamic equilibrium in slowly subducting and not very cold slabs. However, the slab remaining much colder than the normal mantle, the phase boundary of the exothermic transition O → Sp within its limits deflects upward (Fig. 4, *A*), which corresponds to a higher slab density, i.e., a higher negative buoyancy [27–29]. The phase boundary of the endothermic transition Sp → Mw + Pv deflects downward within such slab (Fig. 4, *A*), which yields a slightly lower negative buoyancy. Therefore, under equilibrium conditions, the subducting plate can penetrate straight into the lower mantle (Fig. 4, *A*); its motion becomes faster once it reaches a depth of ~400 km and slower as it sinks deeper than 660 km [29, 30].

The above general setting of phase transformations becomes more complicated in the case of a rapidly subducting thick and cold slab. In this case olivine can long persist as a metastable phase in its relatively colder wedge-shaped core (Fig. 4, *B*). The presence of metastable olivine (MO), which is much less dense than the phase Mw + Pv, makes the lower plate part neutrally or even positively buoyant and thus inhibits its penetration into the lower mantle. As a result, the slab bends upwards, flattens out, and keeps moving in this position along the boundary between the upper and lower mantle as long as the metastable olivine wedge survives (Fig. 4, *B*). The onset of the phase change MO → Sp requires that the temperature reaches some threshold (see the phase diagram in [30, Fig. 1]). The cold slab heats up mostly by conductive heat exchange with the ambient mantle, i.e., relatively slowly. The phase change Sp → Mw + Pv occurs after all metastable olivine has been transformed, which allows the slab to resume sinking into the lower mantle [29, 30].

The distance from the Japan trench to the western end of the flat-lying depth-stagnant slab is 2500 km, of which 1500 km correspond to the slab part within the mantle transition zone (Fig. 1). If the mean annual subduction rate was 9–10 cm/yr [31], the plate could cover this distance in about 25–28 Myr, staying for 15–17 Myr in the transition zone. These estimates are rather close to those predicted in a model which investigates the evolution of subduction in the presence of a metastable olivine wedge for a 110 km initial slab thickness corresponding to an age of 131 Ma (Early Cretaceous) at the point where it enters the subduction zone. According to that model, the time span between the onset of subduction and slab sinking into the lower mantle is about 32 Myr and the stay of the stagnant plate part in the transition zone is about 21 Myr long [30]. Note that the age of the Pacific plate in the region of the Japan trench is just Early Cretaceous [32].

According to seismic tomography, which pretends to have a high resolution, the slab segment we study continues sinking into the lower mantle as deep as the D″ layer. The total length of this slab segment (across strike) from the Japan trench to the D″ layer is about 4500 km. The plate can travel this distance in 45–50 Myr, at a subduction rate of 9–10 cm/yr. If subduction began there in the Jurassic, about 180 Myr ago [22], the entire material of the slab part that penetrated into the lower mantle may have renewed many times.

The slab changes its geometry in the Japan–Izu–Bonin segment when it leaves the zone of stagnation, and it could be thus hypothesized to lose its continuity and sink into the lower mantle in separate pieces [18, 20]. However, the slab apparently remains continuous in the upper mantle (in the asthenosphere and in the transition zone), despite its double kink (Fig. 4, *B*). At the same time, it most likely behaves as a rigid body relative to its environment and can transfer stress. The latter inference is supported by the occurrence of earthquake hypocenters

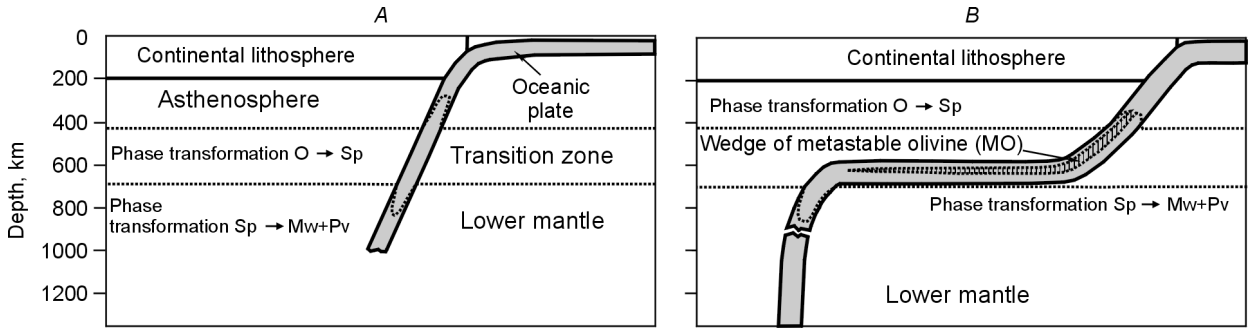

Fig. 4. Sketch of slab subduction. Compiled using [29, 30]. *A* — Moderately cold slab is subducting at slow rate and phase transformations of olivine in it occur under nearly equilibrium conditions; *B* — cold thick slab is subducting rapidly and metastable olivine stays in its core and slab is stagnant in mantle transition zone.

in the stagnant slab part (Fig. 1) as well as by the estimates of its temperature deficit relative to the ambient mantle (see below).

The deflection of the seismic discontinuity corresponding to the transition zone bottom from 660 km indicates a temperature anomaly (difference between the mean temperature of the slab and ambient mantle) of –500 °C beneath the Japan arc [33] and –1100 °C beneath the Izu–Bonin arc [34]. The accuracy of these estimates is as low as ±30% [35]. We take their average value of $\Delta\bar{T}_0 = -800$ °C to represent the temperature anomaly at the starting point of the stagnation zone. The validity of this value is corroborated by numerical modeling of subduction [29, 30].

The temperature anomaly at the endpoint of the stagnation zone after 15–17 Myr decreases to $\Delta\bar{T} = -450...-470$ °C as a result of conductive cooling. The latter estimate was obtained using the equation for an unbounded plate [36]:

$$\Delta\bar{T} = \Delta\bar{T}_0 \cdot \sum_{n=1}^{\infty} \frac{8}{(2n-1)^2\pi^2} \exp\left(-\frac{(2n-1)^2\pi^2}{4}\,\mathrm{Fo}\right),$$

where $\Delta\bar{T}$ is the sought difference between the average (over the thickness) temperature of the plate and its environment after the time t = 15–17 Myr = $4.725\cdot10^{14}$–$5.355\cdot10^{14}$ s; $\Delta\bar{T}_0 = -800$ °C is the initial temperature difference; $\mathrm{Fo} = \chi t/R^2$ is the Fourier criterion; $\chi = 10^{-6}$ m^2/s is the thermal diffusivity; and $2R$ = 120 km = $1.2\cdot10^5$ m is the plate thickness.

The average plate temperature at the endpoint of the stagnation zone increases for 105 °C by frictional heating (see Section 3), i.e., the temperature excess in the slab becomes –345...–365 °C. It is known that the dynamic viscosity of mantle material increases by an order of magnitude at every 100 °C [37]. Therefore, the slab has its viscosity over three orders of magnitude higher than the ambient mantle throughout the stagnant region. With this viscosity contrast, the slab can be interpreted as a rigid body [27].

If the slab disintegrates into pieces in the lower mantle and looses its connection with the stagnant part, its driving force (F_d) must be uniquely due to negative buoyancy in its inclined part in the subduction zone. The flat-lying slab part has a nearly zero buoyancy. The force F_d per unit length of a 120 km thick plate with a dip of 40°, which approaches our conditions, is $5\cdot10^{13}$ N/m [27, 29].

3. STAGNANT SLAB AS A POSSIBLE SOURCE OF PLUME MAGMATISM

According to Ringwood [28], former oceanic crust, in which basalt transforms into eclogite under increasing pressure, experiences small degrees of partial melting between 200 and 600 km during slab subduction. The resultant silicate melts, enriched in incompatible elements because the melting degree is low, react with the ambient depleted mantle above the subducting slab and transform its material into refertilized or fertilized peridotite. The 10–20 km thick layer of fertilized peridotite immediately overlies former oceanic crust and ultimately becomes entrained by the slab sinking. In fact, it integrates into the slab (Fig. 5).

Ringwood's model [28] envisaged that a descending slab breaks up when encounters the 650 km discontinuity (bottom of the transition zone) and its material piles up over the discontinuity making a large "megalith" composed of modified harzburgite with inclusions of former oceanic crust. Basalt in the latter transforms into garnetite after it has lost incompatible elements (Fig. 5). A part of former oceanic crust outside the megalith forms a garnetite layer located immediately over the 650 km discontinuity since garnetite between 650 and 800 km is less dense than the lower mantle. The garnetite layer, which accumulated during that subduction episode as well as throughout the whole Earth's history [28], is of global spread and is physically a thermal boundary layer at base of the upper mantle. Garnetite, as well as the megalith, is overlain by fertilized peridotite (Fig. 5).

As Ringwood hypothesized, an ascending lower mantle flow which may arise at some place over a long time span (say, after 10^7–10^9 years) and be isolated from the upper mantle heats up garnetite and the overlying fertilized peridotite, and the latter thus can rise as plumes. Rising fertilized peridotite is subject to partial melting by decompression at widely varying melting degrees which produce typical plume-related picrites, tholeiites, alkali basalts, basanites, and nephelinites [28].

Recent seismic studies [18–20] and numerical modeling of subduction [30] showed that contrary to Ringwood's idea [28], slabs bear no signature of piling up into a large megalith when colliding with the base of the mantle transition zone but rather either penetrate straight into the lower mantle or become depth-stagnant in the transition zone, remaining apparently continuous. They can also be expected to preserve their stratification, i.e., former oceanic crust overlies modified lithospheric mantle and underlies fertilized peridotite.

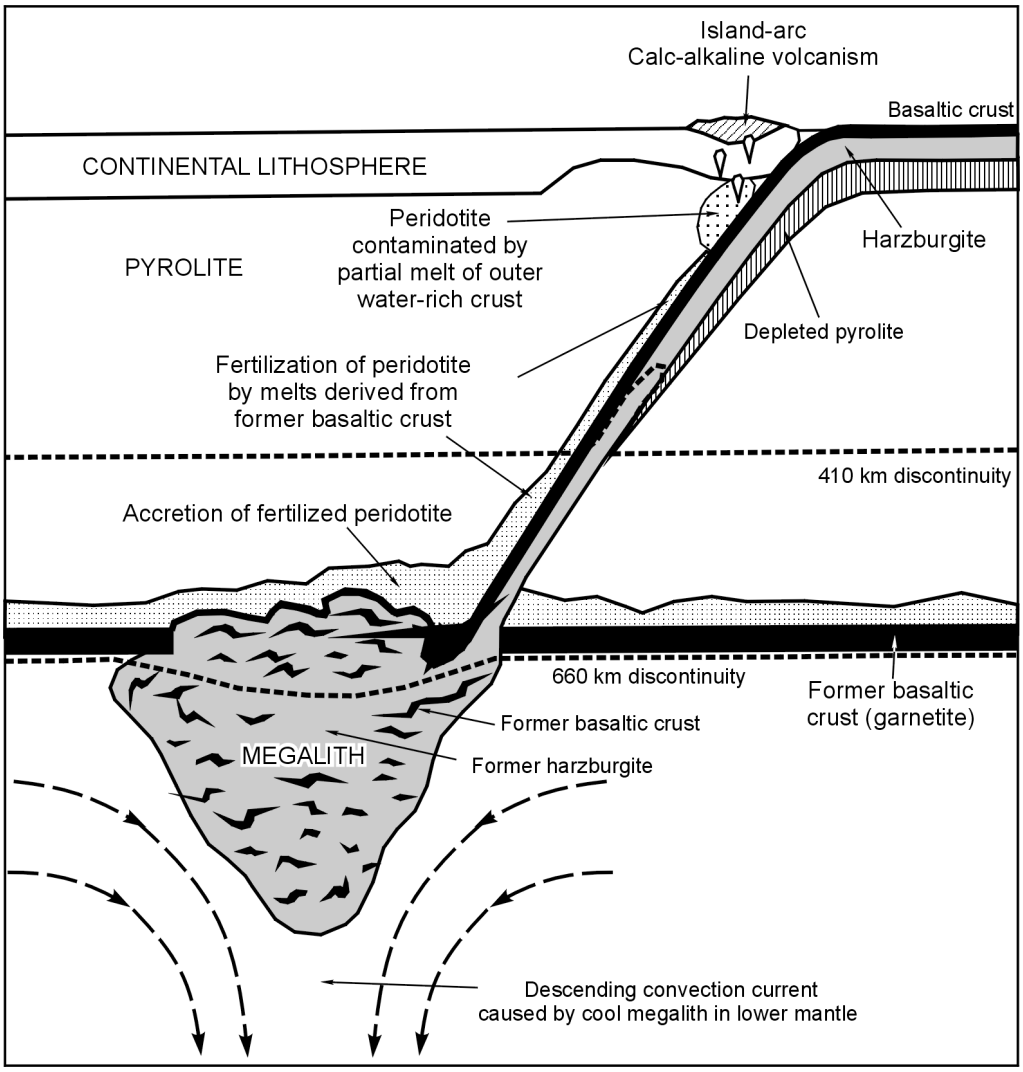

Fig. 5. Model showing structure of mantle and subduction of a cool thick plate of oceanic lithosphere (after [28]).

In principle, olivine in fertilized peridotite should undergo the same phase change as in the slab. If the slab sinks straight into the lower mantle without stagnation, fertilized peridotite should likewise be removed from the transition zone. Yet, fertilized peridotite associated with a depth-stagnant slab continuing its horizontal motion stays in the transition zone for a long time. Its return to the asthenosphere and entrainment into convection requires additional heat sources. In our view, friction at the boundaries of moving plates may be a source of this kind. Friction-related heating in the layer of fertilized peridotite can be estimated approximately proceeding from the following ideas.

Heat generated over a unit area of the boundary of a rigid (see Section 2) plate due to friction is given by [27]:

$$q = \upsilon \cdot \tau, \tag{1}$$

where q is the density of heat release, υ is the plate velocity, τ is the tangential stress at the boundary. As the plate is much colder than ambient mantle, q can be assumed, to a quite good accuracy, to be heat flux into the plate [27].

At a constant subduction rate, the total friction force on both slab boundaries ($2F_{fr}$) and the slab driving force (F_d) are related as $2F_{fr} = -F_d$. We wrote in Section 2 that the force that drives the slab (F_d) is produced by the negative buoyancy of its inclined part in the upper mantle. Thus, we assume the driving force negative in

accordance with negative buoyancy. The force due to the structure of mid-ocean ridge lithosphere is an order of magnitude lower than F_d and can be neglected [27].

Tangential stress at one slab boundary can be found from the relationship between the slab driving force and friction at its two boundaries as

$$\tau = -F_{fr}/L = F_d/2L, \quad (2)$$

where L is the length (across strike) of the slab part where the friction force mainly forms. Experimental data on the relative strength of olivine, garnet, spinel, and perovskite, i.e., minerals assumed to be structural equivalents of those predominant in different mantle zones, suggest that the strength and effective viscosity of rocks in the transition zone are much higher than in the upper and lower mantle [28] (an order of magnitude or more). Therefore, for approximate estimates we can assume that almost all driving force is compensated by friction along the boundaries of the depth-stagnant slab part located within the mantle transition zone.

Substituting (2) into (1) gives

$$q = F_d \upsilon/2L. \quad (3)$$

Assuming that $F_d = 5 \cdot 10^{13}$ N/m (see Section 2), L = 1500 km = $1.5 \cdot 10^6$ m (the length of the depth-stagnant slab part) and $\upsilon = 0.1$ m/yr = $3.17 \cdot 10^{-9}$ m/s, we obtain from (3) that the heat flux into the plate from its top is q = 0.053 W/m^2 = 53 mW/m^2. With the 110–120 km plate being times as thick as the fertilized peridotite layer (10 km), temperature within the latter can be estimated using a model of half-space assuming q to be the heat flux on its surface. On this assumption, the temperature increase ΔT_{fr} is given by [27]

$$\Delta T_{fr}(z, t) = \frac{2q}{k} [\sqrt{\chi t/\pi} \cdot \exp(-z^2/4\chi t) - z/2 \cdot erfc(z/2\sqrt{\chi t})], \quad (4)$$

where *erfc* is the additional error function, k is the thermal conductivity, χ is the thermal diffusivity, z is the distance from the top of the flat-lying slab part to the point where we estimate the temperature increment, and t is the lifetime of heat flux.

We estimate heating in the fertilized peridotite layer at the western endpoint of the flat-lying slab part, i.e., in the place the closest to the plumes we revealed. Therefore, the heat flux lifetime is constrained by the stay of the slab in the stagnation zone (see above for the sense of the notations). Assuming t = 15 Myr = $4.725 \cdot 10^{14}$ s (see Section 2), k = 4 W/(m·K), $\chi = 10^{-6}$ m^2/s [27], at q = 0.053 W/m^2, we obtain from (4) that friction provides heating for $\Delta T_{fr}(0) = 325$ °C at the top of the fertilized peridotite layer and $\Delta T_{fr}(10 \text{ km}) = 210$ °C at its bottom. The increase in the average (over its thickness) temperature of the layer is $\Delta \bar{T}_{fr} = 270$ °C.

The friction-related increase in the average temperature of the whole slab with its thickness $2R$ = 120 km is 105 °C, as follows from the simple relationship $\Delta T_{fr}^{sb} = 2qt/\rho c \cdot 2R$, where $\rho = 4000$ kg/m^3 [27] is the slab density in the transition zone, and c = 1000 J/(kg·deg) [27] is the specific heat. The two in the numerator allows for the friction heat supply through the plate top and bottom. Note that the above temperature estimates remain almost the same at a lower velocity $\upsilon = 0.09$ m/yr in (3), as friction-related heat flux decreases correspondingly but has a longer lifetime.

Anomalously high heat release in exothermic phase transitions of metastable olivine into its high-pressure modifications under disequilibrium conditions can be another source of heating of the stagnant slab (and, hence, fertilized peridotite as well). This source can account for up to 200 °C heating [29].

A temperature increase of 200–300 °C changes the physical properties of fertilized peridotite. Namely, its viscosity becomes two or three orders of magnitude lower [37], i.e., it gains a greater mobility. Its density, which was 4000 kg/m^3 (average density of normal mantle at a depth of 500–650 km [27]) prior to heating, becomes 30–40 kg/m^3 lower, at a thermal expansion coefficient of $3.7 \cdot 10^{-5}$ [30]. As a result, a greater part of less dense fertilized peridotite should detach from the slab sinking into the lower mantle. Batches of fertilized peridotite should rise by buoyancy through the upper part of the transition zone and become involved in asthenospheric convection (Fig. 6).

4. ASTHENOSPHERIC CONVECTION AND PLUMES

Convection cells have roughly equal length and width if convection in a layer depends uniquely on heating of its bottom and cooling of its top [27]. A cold subducting slab is a heat sink for the ambient mantle. Material

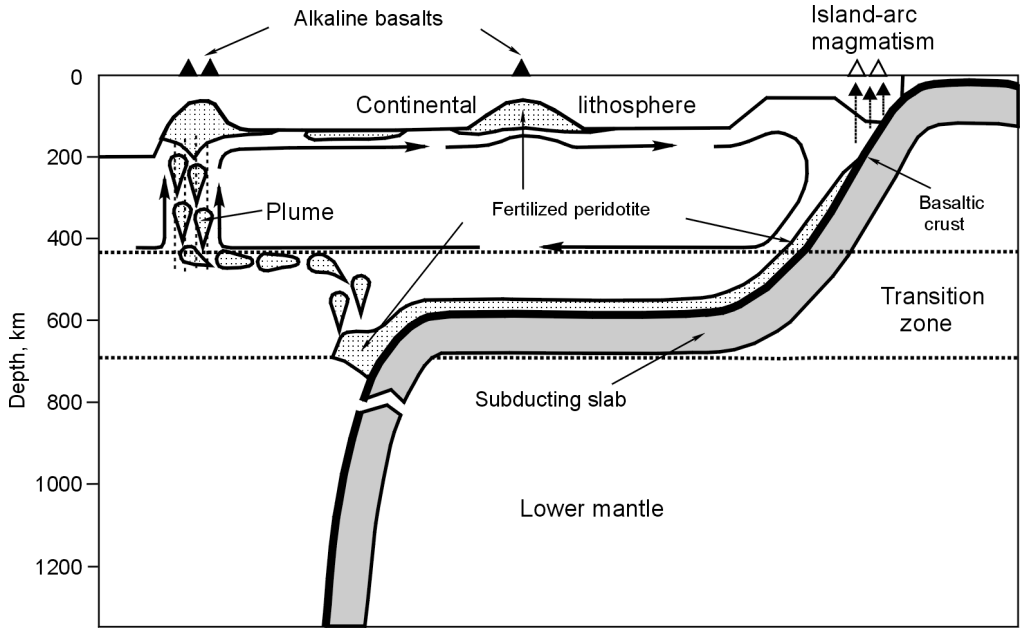

Fig. 6. Suggested formation model of upper mantle plumes. Batches of hot fertilized peridotite detach from depth-stagnant slab during its sinking into lower mantle, rise by buoyancy through the upper part of the mantle transition zone, and become entrained into an elongate asthenospheric convection cell which arises in the asthenosphere cooled by the inclined subducting slab part. Ascending convection flow splits into separate streams which are the upper mantle plumes.

of the convecting mantle layer loses heat near the slab and has to travel a greater distance along the layer bottom in order to heat up enough for acquiring positive buoyancy. This produces horizontally elongate convection cells on both sides of the subducting slab [21, 22], with descending convection flows along the subducting plate. According to estimates based on laboratory experiments, the length of a subcontinental convection cell can reach 3000-4000 km provided that the whole upper mantle is involved in convection [22]. Froidevaux and Nataf [22] hypothesized that an ascending convection flow occurs beneath the Baikal rift. Inasmuch as asthenosphere strongly differs from the mantle transition zone in its mechanic properties (see Section 3), one can expect the existence of independent asthenospheric convection isolated from the mantle below. The length of a subcontinental convection cell was estimated at 2000–3000 km from numerical modeling of asthenospheric convection with regard to the cooling effect of a subducting slab [38]. These estimates remain very approximate because of uncertainty in the parameters that define the convection cell geometry.

The true position of the ascending flow in the convection cell can be inferred from long-wavelength isostatic gravity anomalies. Theoretically, this flow should be marked by gravity lows as relative mass deficit produces positive buoyancy [22]. The zone of gravity lows that runs through the Baikal rift into Central Mongolia and on into Tibet (Fig. 2) may correspond to the ascending flow of asthenospheric convection. The mantle ascending flow tends to split into separate streams [13, 37] which we reveal as three-dimensional bodies corresponding to the tails of upper mantle plumes. Assuming that convection occurs in the asthenosphere, it appears reasonable to prefer the gravity model of plume tails that places their bottom at the asthenospheric base at a depth of 420 km (Fig. 3, *C*).

Note especially that convection should arise in the asthenosphere in the vicinity of the subduction zone whether the slab stagnates or not in the transition zone. However, decompression melting of convecting depleted asthenosphere can produce only MORB-type basalts which melt when asthenospheric material rises to depths of 10–30 km [37]. At the same time, melting in the upper part of convecting depleted asthenosphere in the region we study is hindered because of the thick continental lithosphere varying between 50 and 200 km [39]. Therefore, the streams of the ascending mantle flow free from fertilized peridotite cannot generate magmas in continental environments. Generation of magmas becomes possible only in the presence of fertilized peridotite, and these magmas should have alkali basaltic compositions. Slab stagnation maintains the survival of fertilized peridotite in the upper mantle and its ensuing heating and entrainment into asthenospheric convection (Fig. 6).

The principle possibility for batches of fertilized peridotite to become involved in convection and rise in its ascending flow far distant from the place where they penetrate into the asthenosphere is confirmed by laboratory experiments in which material of small temperature perturbations that arise somewhere at the bottom of convecting mantle rises to the top of the latter in ascending convection flows only [22]. Separate batches of fertilized peridotite are apparently too small for their positive buoyancy to provide their independent relatively rapid ascent without considerable cooling. They can rise to the lithospheric base only when entrained into asthenospheric convection.

The upper mantle plumes we revealed beneath the Baikal rift and mountains of Central Mongolia produce mafic basaltic magmatism just because they are located beyond the edge of the stagnant slab that supplies fertilized peridotite into the asthenosphere, whereas the plumes associated with the ascending convective flow where the slab is not stagnant are amagmatic. For instance, the gravity lows that align with 130° E on the northern extension of the low gravity zone (see the gravity map in [26]) may correspond to the ascending flow beneath the Kuriles-Kamchatka segment of the Pacific plate which does not stagnate in the mantle transition zone [19]. The gravity lows in the south of the region may mark the ascending flow related to subduction of the non-stagnant [19] Philippine Sea plate. No signature of Late Cenozoic volcanism is found within the gravity low centered at 33° N, 107° E (Fig. 2), whereas fields of Late Cenozoic volcanics varying from dacites to andesites, including both alkalic and calc-alkalic varieties [40], are found within the largest gravity low of East Tibet. Judging by the compositions of the volcanics and their association with a long W-E striking fault, this magmatism is related rather to the India-Eurasia collision than to the upper mantle plumes.

Cenozoic mafic alkalic magmas in East Siberia and Central Mongolia were generated at depths estimated at 60 to 110 km [41]. If they were produced by partial melting of fertilized peridotite during its decompression, this magma generation depth corresponds to the conditions of anomalously thin continental lithosphere, i.e., in the asthenospheric upwarps. Asthenospheric upwarps can have been produced by lithosphere heating due to the effect of the plumes. Relatively thin lithosphere may locally persist since pre-Cenozoic stages of the tectonic evolution. Fertilized peridotite apparently can travel long distances in horizontal convection flows and become entrapped in the upwarps (Fig. 6). In both cases, further growth of asthenospheric upwarps to the melting depths of alkali basalts follows the mechanism of gravity instability [10].

According to laboratory experiments, the convection cell elongates (the ascending flow moves off the trench) relatively slowly, at ~2 cm/yr, and not right after the onset of subduction. It takes about 150–200 Myr for a convection cell to reach its stationary position [22], and it is this position that allows plumes to effectively heat up continental lithosphere and develop asthenospheric upwarps. This may be the reason why about 150 Myr elapsed between the start of subduction in the Jurassic and the Late Cenozoic (Late Oligocene) magmatism.

Late Cenozoic magmatism in East Siberia and Central Mongolia included three episodes of high volcanic activity: Late Oligocene, Miocene, and Pliocene-Quaternary [2, 3]. This time discontinuity of volcanism may hardly be related to the behavior of upper mantle convection or to the motion rhythms of the stagnant slab. Both latter processes began in the Jurassic and had stabilized by the Late Cenozoic. The three volcanic episodes most likely were rather induced by changes in the lithospheric permeability under the effect of tectonic pulses associated with changes in far-field stresses.

5. DISCUSSION

As follows from the above consideration, the material of the stagnant slab contributes relatively little to the formation of upper mantle plumes responsible for alkali basaltic magmatism. Silicate melts extracted from partially molten former oceanic crust penetrates to the upper mantle where they are used to produce a layer of fertilized peridotite involved then in the upper mantle convection. The fertilized peridotite can also enrich in fluids during dehydration of the stagnant slab [15, 29]. The main portion of the slab material sinks into the lower mantle as deep as D″ having passed through the zone of stagnation [18].

Both stagnant and non-stagnant segments of subducting oceanic lithosphere that penetrate into the lower mantle belong to downgoing flows of whole-mantle convection. This very convection, in which oceanic lithosphere acts as a thermal boundary layer, is the basic driving mechanism of plate tectonics [13, 27]. The downgoing whole-mantle convection flows are linear due to the presence of rigid plate boundaries, i.e., due to a relatively shallow factor. Following the original idea of Morgan [42], we can assume that the ascending flows of whole-mantle convection are large plumes rising from the lower mantle, such as the Hawaii and Pacific plumes. Their location is not constrained by linear factors which hardly can exist at this depth but is constrained rather by temperature inhomogeneities in the lower mantle at its boundary with the core [14, 38]. The temperature inhomogeneities hold a stable position relative to the mantle. At the same time, material coming from the core can add to the plume material.

Therefore, according to geophysical evidence, whole-mantle convection currently coexists with asthenospheric convection. The two types of convection govern the totality of different tectonic and magmatic events. In convection of both types, the ascending flows split into plumes. In this respect, the modern attempts of interpreting plate motion and plume tectonics separately appear doubtful. Plate motion and plume activity are the two sides of a single process in which many aspects remain unclear and require further studies.

Whole-mantle (lower mantle) plumes are highly productive, i.e., they produce copious volcanism, whereas upper mantle plumes which are responsible for continental magmatism in regions above stagnant oceanic slabs are low productive. The upper mantle plumes may include Late Cenozoic plumes of Central Europe [43] besides the plumes we discussed.

Lower mantle plumes differ from upper mantle plumes also in their relatively fixed position in the absolute coordinates, whereas the position of plumes in the upper mantle controlled by the lateral extent of asthenospheric convection cells remains stable relative to the subduction zone and, hence, relative to the moving continental lithosphere. The fields of Cenozoic alkali basalts of different ages (Late Oligocene, Miocene, and Pliocene-Quaternary) in East Siberia and Central Mongolia either nearly coincide or are closely spaced, and their spacing is beyond any comparison with the distance Eurasia has traveled through the Cenozoic. Moreover, the migration of volcanic fields in some cases disagrees with the direction of the continent motion [10] and may be due to propagation of faults in the lithosphere.

Note that volcanics associated with both high and low productive plumes are very similar in chemistry. This geochemical convergence can be primarily accounted for by the fact that in both cases magmas melt at similar depths from rising hot mantle largely composed of material supplied from the former oceanic crust of subducted plates. According to isotope ratios, formation of isotope-bearing minerals that belong to former oceanic crust and magma generation are separated by quite a long time span [7, 28]. This fact is often interpreted as evidence of the lower mantle origin of plume material as the latter is assumed to contain recycled old oceanic crust which must have reached the D″ depth very long ago and stay there till later thermal activity. This hypothesis appears quite plausible. However, another plausible assumption may be, in some cases, that isotope-bearing minerals belonged to old continental lithosphere whose pieces were entrained by a subducting plate relatively recently. In our case, the lithosphere beneath the Japan arc is of Precambrian age [25]. It appears quite probable that the capture of its fragments is responsible for the $^{143}Nd/^{144}Nd$ ratios in some basalt samples from Central Mongolia reaching 0.5121 ($\varepsilon_{Nd} = -10$) [41]. Large ε_{Nd} variations (from +3 to –10) in different basalt samples of the same chemistry [41] is evidence rather of the local presence of ancient minerals in the subducting plate than of its general very old age.

CONCLUSIONS

The reported geophysical data and their interpretation, along with the available evidence of the upper mantle composition, allow the following inferences.

The zone of upper mantle plumes we revealed [8–10] and the related alkali basalt fields the most distant from the Pacific subduction are located beyond the western edge of the depth-stagnant oceanic slab segment advanced the farthest beneath the continent.

Following Ringwood [28], we believe that magmas related to upper mantle plumes are derived from refertilized peridotite which forms at depths between 200 and 600 km under the effect of melts produced by partial melting of subducting oceanic crust on the overlying depleted mantle.

We suppose that the layer of fertilized peridotite integrates into the slab, becomes involved in its motion, and heats up either by friction at the top of the moving plate while it stays within the stagnation zone or by latent crystallization heat released in phase change of metastable olivine under disequilibrium conditions. Batches of hot fertilized peridotite detach from the slab during its sinking into the lower mantle, rise by buoyancy through the upper part of the mantle transition zone and become entrained into the elongate convection cell which arises in continental asthenosphere cooled at the contact with the inclined subducting slab. The ascending convection flow splits into separate streams which are exactly the upper mantle plumes. Fertilized peridotite experiences partial melting by decompression during its rise, which produces the whole diversity of mafic alkalic magmas typical of intracontinental volcanism.

We wish to thank D. Zhao who kindly offered digital global seismic tomography data. The paper profited much from constructive criticism by V.V. Yarmolyuk and O.P. Polyansky.

The study was supported by grants 03-05-64036, 05-05-64477, and 05-05-97260 from the Russian Foundation for Basic Research.

REFERENCES

1. Zorin, Yu.A., V.M. Kozhevnikov, M.R. Novoselova, and E.Kh. Turutanov, Thickness of the lithosphere beneath the Baikal rift zone and adjacent regions, *Tectonophysics*, **168**, 327–337, 1989.

2. Rasskazov, S.V., Hot spot and structure of the Western Baikal Rift System, *Geologiya i Geofizika (Soviet Geology and Geophysics)*, **32**, 9, 72–80(63–70), 1991.

3. Logatchev, N.A., and Yu.A. Zorin, Baikal rift zone: structure and geodynamics, *Tectonophysics*, **208**, 273–286, 1992.

4. Dobretsov, N.L., M.M. Buslov, D. Delvaux, N.A. Berzin, and V.D. Ermikov, Meso- and Cenozoic tectonics of the Central Asian mountain belt: Effects of the lithospheric plates interaction and mantle plumes, *Intern. Geol. Rev.*, **38**, 430–466, 1996.

5. Grachev, A.F., Khamar-Daban — a hotspot in the Baikal rift: evidence from chemical geodynamics, *Izv. RAN. Ser. Fizika Zemli*, 3, 3–28, 1998.

6. Rasskazov, S.V., N.A. Logachev, I.S. Brandt, S.B. Brandt, and A.V. Ivanov, *Late Cenozoic geochronology and geodynamics (Southern Siberia—Southern and Eastern Asia)* [in Russian], 288 pp., Nauka, Novosibirsk, 2000.

7. Yarmolyuk V.V., V.G. Ivanov, V.I. Kovalenko, and B.G. Pokrovsky, Magmatism and geodynamics of the South Baikal volcanic province (mantle hotspot), from geochronological, geochemical, and isotope (Sr, Nd, O) data, *Petrologiya*, **11**, 1, 3–34, 2003.

8. Zorin, Yu.A., E.Kh. Turutanov, V.V. Mordvinova, V.M. Kozhevnikov, T.B. Yanovskaya, and A.V. Treusov, The Baikal rift zone: the effect of mantle plumes on older structure, *Tectonophysics*, **371**, 153–173, 2003.

9. Zorin, Yu.A. and E.Kh. Turutanov, Regional isostatic gravity anomalies and mantle plumes in southern East Siberia (*Russia*) and Central Mongolia, *Geologiya i Geofizika (Russian Geology and Geophysics)*, **45**, 10, 1248–1258(1200–1209), 2004.

10. Zorin, Yu.A., and E.Kh. Turutanov, Plumes and geodynamics of the Baikal rift zone, *Russian Geology and Geophysics (Geologiya i Geofizika)*, **46**, 7, 669–682(685–699), 2005.

11. Grachev, A.F., Mantle plumes and geodynamics, *Vestnik OGGGGN RAN*, 5, 129–158, 1998.

12. Parmentier, E.M., D.L. Turcotte, and K.E. Torrance, Numerical experiment on the structure of mantle plumes, *J. Geophys. Res.*, **80**, 4417–4424, 1975.

13. Malamud, B.D., and D.L. Turcotte, How many plumes are there?, *Earth Planet. Sci. Lett.*, **174**, 113–124, 1999.

14. Zhao, D., Seismic structure and origin of hotspots and mantle plumes, *Earth Planet. Sci. Lett.*, **192**, 251–265, 2001.

15. Zhao, D., J. Lei, and R. Tang, Origin of the Changbai intra-plate volcanism in Northeast China: Evidence from seismic tomography, *Chinese Science Bulletin*, **49**, 13, 1401–1408, 2004.

16. Rasskazov, S., H. Taniguchi, A. Goto, and K.D. Litasov, Magmatic expression of plate subduction beneath East Asia in the Mesozoic through Cenozoic, *Northeast Asian Studies*, **9**, 179–219, 2005.

17. Fukao, Y., M. Obayashi, H. Inoue, and M. Nebai, Subducting slabs stagnant in the mantle transition zone, *J. Geophys. Res.*, **97**, 4809–4822, 1992.

18. Bijwaard, H, W. Spakman, and E.R. Engdahl, Closing the gap between regional and global travel time tomography, *J. Geophys. Res.*, **103**, 30,055–30,078, 1998.

19. Gorbatov, A., and B.L.N. Kennett, Joint bulk-sound and shear tomography for Western Pacific subduction zones, *Earth Planet. Sci. Lett.*, **210**, 527–543, 2003.

20. Zhao, D., Global tomographic images of mantle plumes and subducting slabs: insight into deep Earth dynamics, *Physics of the Earth and Planetary Interiors*, **146**, 3–35, 2004.

21. Rabinowicz, M., B. Lago, and C. Froidevaux, Thermal transfer between the continental asthenosphere and the oceanic subducting lithosphere: its effect on sub-continental convection, *J. Geophys. Res.*, **85**, 1838–1853, 1980.

22. Froidevaux, C., and H.C. Nataf, Continental drift: what is driving mechanism?, *Geologische Rundschau*, **70**, 166–176, 1981.

23. Gorbatov, A., S. Widiyantoro, Y. Fukao, and E. Gordeev, Signature of remnant slabs in the North Pacific from P-wave tomography, *Geophys. J. Intern.*, **142**, 27–36, 2000.

24. Gudmundsson, O. and M. Sambridge, A regionalized upper mantle (RUM) seismic model, *J. Geophys. Res.*, **104**, 28,803–28,812, 1998.

25. Parfenov, L.M., N.A. Berzin, A.I. Khanchuk, G. Badarch, V.G. Belichenko, A.N. Bulgatov, S.I. Dril', G.L. Kirillova, M.I. Kuz'min, W. Nockleberg, A.V. Prokop'ev, V.F. Timofeev, O. Tomurtogoo, and H. Yan,

A formation model of orogenic belts in Central and Northeastern Asia, *Tikhookeanskaya Geologiya*, **22**, 6, 7–41, 2003.

26. Kaban, M.K., P. Schwintzer, and S.A. Tikhotsky, A global isostatic gravity model of the Earth, *Geophys. J. Intern.*, **136**, 519–536, 1999.

27. Turcotte, D.L., and G. Schubert, *Geodynamics: Applications of continuum physics to geological problems*, 450 pp., J. Wiley & Sons, New York, 1982.

28. Ringwood, A.E., Phase transformations and their bearing on the constitution and dynamics of the mantle, *Geochim. Cosmochim. Acta*, **55**, 8, 2083–2110, 1991.

29. Bina, C.R., S. Stein, F.C. Marton, and E.M. Van Ark, Implications of slab mineralogy for subduction dynamics, *Physics of the Earth and Planetary Interiors*, **127**, 51–66, 2001.

30. Tetzlaff, M., and H. Schmeling, The influence of olivine metastability on deep subduction of oceanic lithosphere, *Physics of the Earth and Planetary Interiors*, **120**, 29–38, 2000.

31. Miller, M.S., A. Gorbatov, and B.L.N. Kennett, Heterogeneity within the subducting Pacific slab beneath the Izu–Bonin–Mariana arc: Evidence from tomography using 3D ray tracing inversion techniques, *Earth Planet. Sci. Lett.*, **235**, 331–342, 2005.

32. Müller, R.D., W.R. Roest, J.-Y. Royer, L.M. Gahagan, and J.G. Sclater, Digital isochrons of the world's ocean floor, *J. Geophys. Res.*, **102**, 3211–3214, 1997.

33. Li, X., S.V. Sobolev, R. Kind, X. Yuan, and Ch. Estabrook, A detailed receiver function image of the upper mantle discontinuities in the Japan subduction zone, *Earth Planet. Sci. Lett.*, **183**, 527–541, 2000.

34. Castle, J.C., and K.C. Creager, Topography of the 660-km seismic discontinuity beneath Izu–Bonin: Implications for tectonic history and slab deformation, *J. Geophys. Res.*, **103**, 12,511–12,528, 1998.

35. Vidale, J.E., and H.M. Benz, Upper-mantle seismic discontinuities and thermal structure of subduction zones, *Nature*, **356**, 678–683, 1992.

36. Lykov, A.V., *The theory of thermal conductivity* [in Russian], 392 pp., Gostekhteoretizdat, Moscow, 1952.

37. White, R., and D. McKenzie, Mantle plumes and flood basalts, *J. Geophys. Res.*, **100**, 17,543–17,585, 1995.

38. Dobretsov, N.L., A.G. Kirdyashkin, and A.A. Kirdyashkin, *Deep geodynamics* [in Russian], 407 pp., Nauka, Novosibirsk, Filial GEO, 2001.

39. Zorin, Yu.A., T.V. Balk, M.R. Novoselova, and E.Kh. Turutanov, Lithospheric thickness beneath the Mongolia-Siberia mountainous province and its surroundings, *Izv. AN SSSR. Ser. Fizika Zemli*, 7, 33–42, 1988.

40. Whitford-Stark, J.L., A survey of Cenozoic volcanism on mainland Asia, *Geol. Soc. Amer. Special Pap.*, **213**, 1–74, 1987.

41. Ivanov, A.V., One rift, two models, *Science First Hand*, 1 (September), 50–61, 2004.

42. Morgan, W.J., Deep mantle convection plumes and plate motions, *Amer. Assoc. Petrol. Geol. Bull.*, **56**, 203–213, 1972.

43. Granet, M., M. Wilson, and U. Achauer, Imaging a mantle plume beneath the French massif Central, *Earth Planet. Sci. Lett.*, **136**, 281–296, 1995.

Editorial responsibility: V.A. Vernikovsky Received 1 June 2004